

HFGD: High-level Feature Guided Decoder for Semantic Segmentation

Ye Huang¹ Di Kang² Shenghua Gao³ Wen Li¹ Lixin Duan^{1*}

¹ University of Electronic Science and Technology of China

² Tencent AI LAB

³ ShanghaiTech University

edward.ye.huang@qq.com

Abstract

Commonly used backbones for semantic segmentation, such as ResNet and Swin-Transformer, have multiple stages for feature encoding. Simply using high-resolution low-level feature maps from the early stages of the backbone to directly refine the low-resolution high-level feature map is a common practice of low-resolution feature map upsampling. However, the representation power of the low-level features is generally worse than high-level features, thus introducing “noise” to the upsampling refinement. To address this issue, we proposed High-level Feature Guided Decoder (HFGD), which uses isolated high-level features to guide low-level features and upsampling process. Specifically, the guidance is realized through carefully designed stop gradient operations and class kernels. Now the class kernels co-evolve only with the high-level features and are reused in the upsampling head to guide the training process of the upsampling head. HFGD is very efficient and effective that can also upsample the feature maps to a previously unseen output stride (OS) of 2 and still obtain accuracy gain. HFGD demonstrates state-of-the-art performance on several benchmark datasets (e.g., Pascal Context, COCOStuff164k, and Cityscapes) with small FLOPs. The full code will be available at <https://github.com/edwardyehuang/HFGD.git>.

1. Introduction

Semantic Segmentation is a fundamental task in computer vision, requires densely predicted class labels for every pixel of the input image. Rapid progresses [25, 31, 53, 3, 4, 45, 43, 50, 5, 52, 9, 55, 21, 18, 17, 44, 16, 15] have been witnessed since the existence of fully convolutional networks (FCNs) [25], which makes dense prediction tasks much more efficient than before. Most methods consist of an *encoder* used to extract coarse (i.e. low-resolution) high-

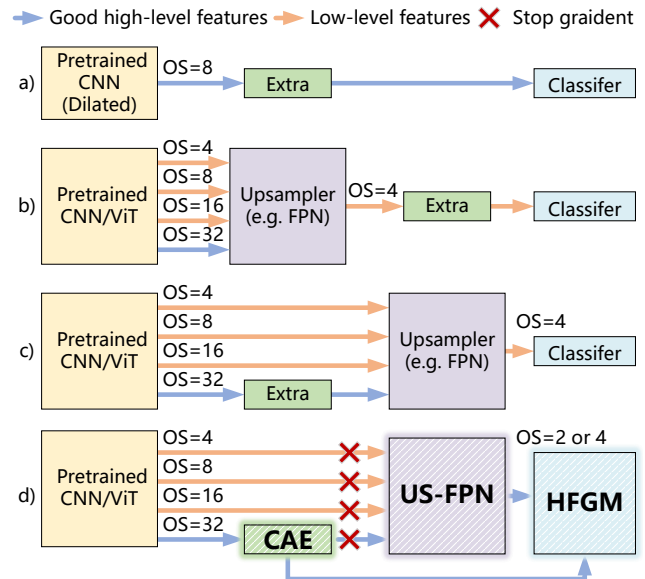


Figure 1: Comparison between our method (d) and existing methods (a/b/c). Our method proposes to take full use of the better high-level pretrained features (i.e. CAE) to guide (i.e. HFGM) the upsampling process (U-SFPN), achieving better accuracy while using much less computation. Blue arrows in the figure represent “good” high-level features that are more ready for final classification while orange arrows represent low-level features that exist a substantial gap to the task and thus possibly being “noisy”.

level abstract features and a *decoder* used to compensate lost spatial details from high-resolution low-level features.

Most commonly, the backbone encoder is pretrained on large-scale image classification dataset (e.g. 1.2M labeled training images in ImageNet-1k) since semantic segmentation is essentially a per-pixel classification task. However, the classification backbones usually produce feature maps in an output stride of 32 ($OS = 32$), which is too coarse for accurate and detailed (e.g. object boundaries, thin/small objects). So investigating stronger and more efficient up-

*Corresponding author

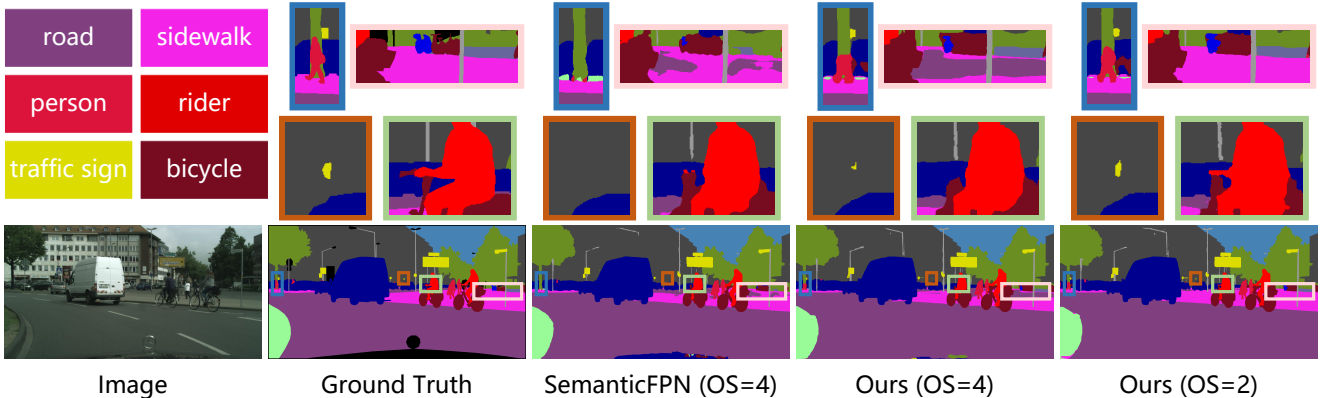


Figure 2: Demonstration of the impact of producing higher-resolution feature maps on Cityscapes. All the results are predicted using single-scale without flipping protocol. ResNet-50 is used as the backbone.

sampler has been one major direction in recent years.

Existing approaches can be roughly classified into two categories, including dilation-based methods that stop further reducing feature map resolution after several stages (e.g. $OS = 8$) and pyramid-based methods that use learned upsampler to gradually fuse multi-resolution feature maps from $OS = 32$ to $OS = 4$. Dilated CNNs [4, 40, 55, 18, 49, 17, 16] better utilize the “good” pretrained backbone features and usually result in faster convergence and better accuracy, but at the cost of huge computation overhead. pyramid-based methods are more efficient but not as effective as their dilated counterparts [19, 22, 31] even with $OS = 4$ feature maps. We conclude that, during the training of the new upsampling head, the “good” high-level backbone features are negatively affected by the “noisy” low-level features (since there exists a big gap between the low-level features and the final classification features) and the randomly initialized weights in the head.

Thus, we propose to make better use of the “good” high-level backbone features by 1) protecting them from the updating of the upsampling header and 2) further using them to guide the learning of the upsampling head. Specifically, the *protection* is realized by stopping gradients from back-propagating through the upsampling header to the backbone and the *guidance* is realized by reusing the class kernels (i.e. the final classification layer) learned along with the coarse high-level features in the upsampling head (See. Fig. 1d). Since the coarse high-level features play a crucial role in our framework, We further explored different extra encoding modules to improve them, resulting in our context-augmented encoder (CAE). Note that we can use strong encoding modules (such as ASPP, full self-attention) without introducing too much computational overhead since the resolution of the high-level feature maps is low. Lastly, we propose an ultra SemanticFPN (U-SFPN) based on the widely-used SemanticFPN (SFPN) to obtain better representation

as our upsampling head. Due to the efficiency and effectiveness of our framework, we can upsample the feature maps to an unseen size of $OS = 2$ and still achieve accuracy gain see Fig. 2, Fig. 5 and Tab. 8).

In summary, our contributions in this work include:

1. Our proposed HFGD is a novel guided upsampling paradigm for FPN like upsampler and can effectively and efficiently use good high-level coarse features to guide the learning of the upsampling head.
2. We propose a powerful context-augmented encoder based on CAR [15] for the coarse ($OS = 32$) guiding features, resulting in better accuracy with small computation overhead.
3. We propose U-SFPN to obtain better and higher-resolution feature maps of $OS = 2$.
4. HFGD achieves state-of-the-art accuracy (e.g. 64.9% mIOU on Pascal Context) while being efficient among methods with backbones that only use ImageNet data for pretraining and without use more technique [36].

2. Related works

ImageNet pretrained backbones. Due to limited training data¹, semantic segmentation methods usually use backbone networks pretrained on large-scale image classification datasets (e.g. 1.2M images in ImageNet-1K, 14M in ImageNet-21K). If not using pretrained backbones (i.e. trained from scratch), there still exists a substantial performance gap even with much more training epochs. For example, we can only get 37% mIOU (vs 47% using pretrained weights) if we train a classic FCN with ResNet-50 backbone from scratch after 4 times number of training iterations on Pascal Context. Using a backbone pretrained on

¹So far the largest semantic segmentation data is COCOStuff [1] that contains 118K training images. There are only 4.9K training images in Pascal Context [28] and 2.9K training images in Cityscapes [26].)

image classification task is particularly helpful for semantic segmentation because these two tasks are closely related and the scale of the classification dataset is at least one order of magnitude larger than that of the semantic segmentation dataset. However, most of the popular backbones finally produce feature maps with an output stride (OS) size of 32, including VGG [34], ResNet [13], EfficientNet [27], Swin [23], etc. Thus, dilated convolutions or an upsampling head is required to recover the lost spatial information for the $OS = 32$ feature maps.

Dilated convolutions. Dilated CNNs [2, 46] usually use dilated convolutions layers starting from $OS = 8$ feature maps, resulting in the constant resolution thereafter (see Fig. 1a). Since the resolution is not very coarse, only some extra feature encoding layers are introduced to obtain context-augmented features (but still operated in $OS = 8$) before the final logit regression. Dilation models are easy and fast to train since only a few randomly initialized weights are appended to the well-trained high-level backbone features. However, the computation cost for the final layers increases quadratically with the feature map width. Another issue is that dilation is only applicable for CNN backbones [34, 13, 6, 32, 51, 39, 24] but not for Transformer-based backbones [8, 23].

Pyramid-based upsampling head. Another popular strategy adopts upsampling head, such as UNet [31], FPN [22], SemanticFPN [20], Uper [43] and JPU [42] (see Fig. 1b&c). They upsample the $OS = 32$ feature map to the $OS = 4$ feature map without using dilated convolutions layers, resulting in much less computation cost². To better restore the lost spatial details in the $OS = 32$ high-level feature maps, upsampling heads often progressively merge features from different stages of the backbone network (i.e. a feature pyramid) into the upsampled high-level feature maps.

However, the accuracy of these upsampling methods are usually not as good as dilated CNNs since they introduce more randomly initialized weights, especially those weights used to process early-stage low-level features mainly due to two reasons. Firstly, the new learnable weights are trained only with semantic segmentation data that are at least an order of magnitude smaller than ImageNet. Secondly, updating early-stage backbone features (low-level features) with such small amount of data could easily lead to negative effects (e.g. bad generalization).

Extra context encoding modules. Many powerful feature enhancement techniques have been proposed, including pyramid pooling module (PPM) [53], atrous spatial pyramid pooling (ASPP) [3], Self-Attention [40, 9], etc. Most of these modules fuse pixel features from different locations from the same layer (i.e. context information).

²Lightweight decoders intentionally avoid convolution layers on feature maps that are in high-resolution and contains many channels simultaneously.

For dilated CNNs (Fig. 1a), they are applied between the backbone and the output logits. For upsampling-based models (Fig. 1b&c), these extra encoding modules could be applied either before (i.e. on low-resolution feature maps) or after the upsampler (i.e. on high-resolution feature maps). Their accompanied extra computation cost could be huge (e.g. full self-attention) when applied on the high-resolution feature maps. In our method, we insert these extra encoding modules before the upsampler (see CAE in Fig. 1d) because we use the high-level coarse features as guidance of the upsampler. More accuracy gain could be obtained if the high-level coarse features are better. In fact, we can freely use as powerful as possible extra encoding module for our CAE since it operates on low-resolution feature maps.

3. Proposed Method

To achieve a good balance between accuracy and efficiency, our proposed High-level Feature Guided Decoder (HFGD) adopts a computationally more efficient upsampling strategy but can better utilize the good high-level coarse features to guide the training process of the upsampling head (i.e. HFGM in Sec. 3.1). Since the high-level coarse features play a crucial role, HFGD first improve the high-level coarse feature maps using a novel context-augmented encoder (CAE, in Sec. 3.2). Lastly, we make some modifications based on SemanticFPN [19] and propose Ultra SemanticFPN (U-SFPN, in Sec. 3.3). generates an accurate low-resolution feature map without using a dilated backbone to save computation.

3.1. High-level feature guided module (HFGM)

Motivation. The last stage high-level features extracted from a backbone are already “good” representations for semantic segmentation since segmentation is essentially a per-pixel classification task. However, the high-level features are too coarse ($OS = 32$) for accurate segmentation.

In contrast, the features from the earlier stages are in higher resolution and contains more detailed information, and thus suitable for compensating the lost spatial details. However, there exists a substantial gap between low-level backbone features and the final segmentation feature. Different from previous FPN-like methods that equally treat the high-/low-level during the fusing stage in the upsampling head, we propose to only “trust” the high-level features and use them as guidance for the upsampling head.

Implementation. We realize the aforementioned idea with properly stopped gradients (see Fig. 3). The stop gradient operation inside HFGM ensures the class kernels are updated only according to the right path (i.e., high-level coarse features on $OS = 32$). The stop gradient operations on $OS = n$ paths (between U-SFPN and CAE / backbone) protect well-trained backbone features from being negatively

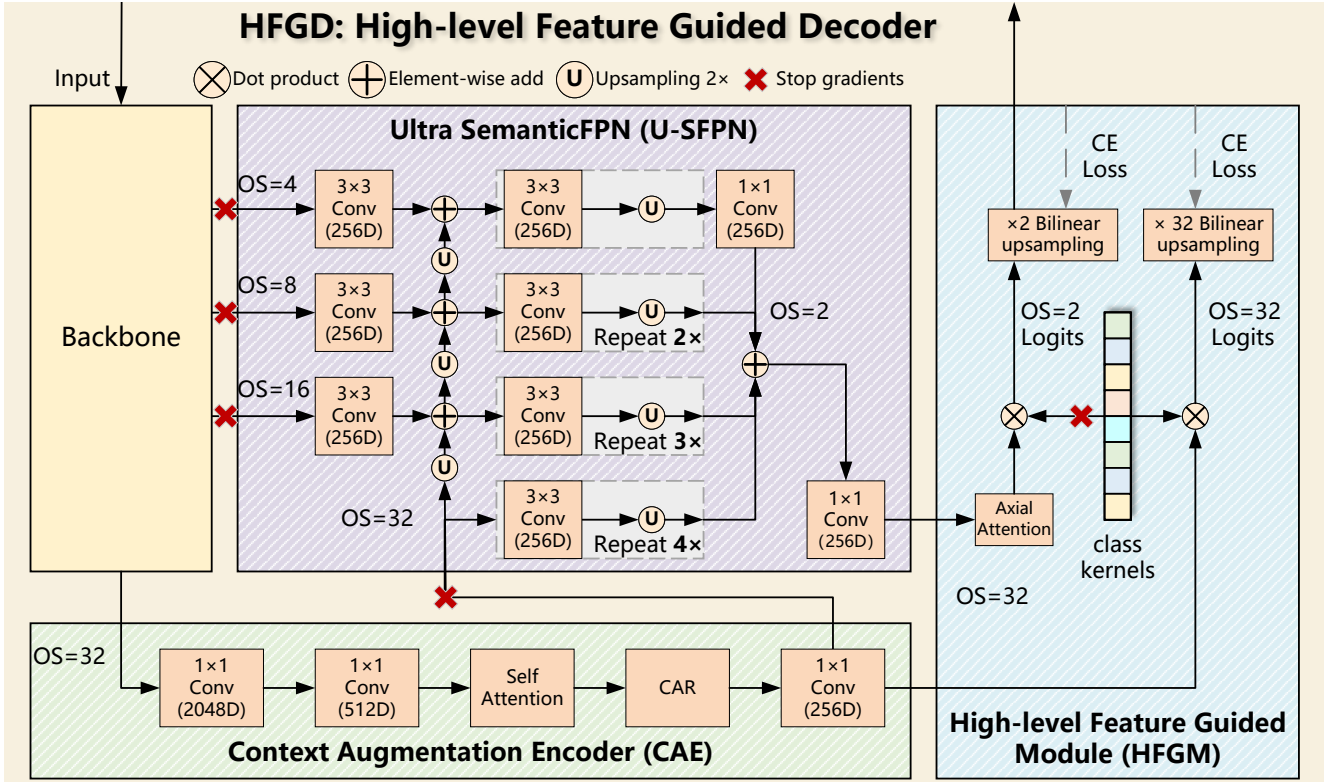


Figure 3: Architecture of the proposed high-level feature guided decoder (HFGD). HFGD consists of three components: a context augmentation encoder (CAE) that generates accurate pixel representations, an ultra SemanticFPN (U-SFPN) that produces high-resolution feature maps, and a high-level feature guided module (HFGM) that guides the upsampling process in U-SFPN. With carefully designed stop gradient operations (i.e. the red crosses ✖), the the class kernels will co-evolve with the CAE branch during training and guide the learning of the U-SFPN branch. See Sec. 3.1 for details.

affected by the noisy gradients from the randomly initialized upsampling head.

With these stop gradient operations, the class kernels are trained to cooperate with the “good” high-level CAE features and transform a 256-D pixel representation to class probabilities. The class kernels guide the training of the upsampler because the weights in the upsampler adapt according to the class kernels (note the stop gradient operation inside HFGM) but not vice versa. As a result, pixel representations from the upsampler are forced to approaching their corresponding pixel representations from CAE. In this way, the class kernels are free from noisy gradient (especially in the early training epochs) from its left path and guide the learning of the upsampling head (e.g. U-SFPN).

Another small but very helpful operation is the inclusion of an axial attention [14, 38, 16] layer. This axial attention broadcasts the gradient of one pixel to all spatial locations, resulting in further improvement (see Tab. 2). In consideration of computation, we choose axial attention [14] instead of full self-attention for spatial context augmentation since the resolution of the path is high (e.g. $OS = 2$ or 4).

The computation difference between axial attention and full self-attention is huge for high-resolution input [14, 38, 16].

3.2. Context-augmented encoder (CAE)

We propose a context-augmented encoder to achieve further improvement since the coarse high-level features are used as guidance and play a crucial role in our HFGD. Note that the resolution of this path is low (i.e. $OS = 32$), we can freely use any powerful modules (e.g. ASPP [4, 5], PPM [53], OCR [47] and full self-attention [40, 37, 52]) without introducing too much computation.

In our experiments, we find using CAR [15] based CAE brings most accuracy gain (see Tab. 1). Specifically, our CAE contains two leading convolution layers to transform the backbone features to 512-D, followed by a full self-attention layer [40] regularized by class-aware regularizations (CAR) [15] and a trailing convolution layer. Note that using 1×1 conv layers is much better than 3×3 conv layers (50.76% vs 50.42%) in CAE possibly due to that the receptive field size of every pixel is large enough. Using two consecutive convolutions layers is better, possibly due

to increased capacity, so that the training on segmentation data can focus more on updating these new weights without modifying the backbone weights too much.

3.3. Ultra SemanticFPN (U-SFPN)

For the upsampling head, we propose Ultra SemanticFPN (U-SFPN) based on SemanticFPN (SFPN) [19] with the following three modifications. Since our upsampling training is more effective, we can keep upsampling to an even higher resolution (i.e. $OS = 2$) with better accuracy (79.81% vs 79.11% mIOU using ResNet-50 backbone on Cityscapes)³.

To achieve this goal, we include one more “conv-upsample” block for every branch to get $OS = 2$ feature maps. Note that we did not use $OS = 2$ low-level features from the backbone since some recent backbones (e.g. Swin [23], ConvNeXT [24]) do not have an $OS = 2$ feature map (directly downsampled to $OS = 4$). Secondly, we change the leading 1×1 conv to 3×3 conv layers since it can collect more spatial information to correct potential “noise” in the low-level features. Thirdly, we increase the channel numbers from 128 to 256 since we find it is beneficial for obtaining more accurate and detailed results.

4. Training details

For fair comparison, we use the same training settings (listed below) for all the ablation studies and the experiments to compare with the other state-of-the-art methods unless specified.

Settings	Ablation studies	SOTA experiments
Batch size	16	16
Optimizer	SGD	AdamW
Learning rate decay	<i>poly</i>	<i>poly</i>
Initial Learning rate	0.01	0.00004
Weight decay	0.0001	0.05
Photo Metric Distortion	-	✓
Batch Norm Decay	0.9997	0.9997
Sync Batch Norm	✓	✓
Layer Norm epsilon	1e-6	1e-6
Mixed precision	✓	✓

5. Experiments on Pascal Context Dataset

The Pascal Context dataset contains 4,998 training images and 5,105 testing images. Following the common practice, we use its 59 semantic classes to conduct the ablation studies and experiments. Unless specified, we train the models on the training set for 30K iterations for ResNet backbone and 40K for Swin-Large and ConvNeXt-Large.

³We only test $OS = 2$ results on Cityscapes since the ground truth annotations on other datasets (e.g. Pascal Context) are not as accurate.

5.1. Ablation studies on CAE

We first conduct ablation studies on CAE in Tab. 1 since we use the high-level coarse features to guide the training of the upsampling head. Our CAE design surpasses the other alternatives by a substantial margin, with and without SemanticFPN [19].

Backbone	Upsampling	Extra Encoding	mIOU(%)
ResNet-50	-	Identity	45.87
ResNet-50	SFPN	Identity	47.14
ResNet-50	-	ASPP [5]	46.41
ResNet-50	SFPN	ASPP [5]	47.81
ResNet-50	-	OCR [47]	45.50
ResNet-50	SFPN	OCR [47]	47.39
ResNet-50	-	Self-Attention [40]	45.02
ResNet-50	SFPN	Self-Attention [40]	45.90
ResNet-50	-	Ours	47.35
ResNet-50	SFPN	Ours	48.76

Table 1: Ablation studies on different CAE settings on Pascal Context dataset. Experiments without upsampling head produces $OS = 32$ feature maps while those with SemanticFPN (S-FPN) [19] produces $OS = 4$ feature maps.

5.2. Ablation studies on HFGM

In Tab. 2, we evaluate the effectiveness of our proposed HFGM. The upsampling head is fixed to SemanticFPN and the CAE part is fixed to our design. HFGM without axial attention improves mIOU by 0.46% while HFGM with axial attention improves mIOU by 1.52%. Axial attention can efficiently broadcast the effect of HFGM to all spatial locations (also see Sec. 3.1 for more discussion).

Backbone	Upsampling	CAE	HFGM	mIOU(%)
ResNet-50	SFPN	Ours	-	48.76
ResNet-50	SFPN	Ours	w/o AA	49.22 (+0.46)
ResNet-50	SFPN	Ours	✓	50.28 (+1.52)

Table 2: Ablation studies on different HFGM settings on Pascal Context dataset. HFGM effectively improves the accuracy, especially when it contains an axial attention (AA) layer since AA can effectively back-propagate the guidance signal from the good high-level features (i.e. output of CAE) to all spatial locations, resulting in more accurate upsampled feature representations.

5.3. Ablation studies on U-SFPN

In Tab. 3, we conduct ablation studies on U-SFPN to verify the effectiveness of our improved version of SFPN with

fixed CAE and HFGM. Replacing SFPN with U-SFPN improves the mIOU of ResNet-50 (CAE + HFGM) by 0.48%, reaching 50.76%. The improvement is even larger (1.14%) when using Swin-Large as the backbone.

Backbone	CAE	HFGM	Upsampling	mIOU(%)
ResNet-50	Ours	✓	SFPN	50.28
ResNet-50	Ours	✓	U-SFPN	50.76 (+0.48)
Swin-Large	Ours	✓	SFPN	59.32
Swin-Large	Ours	✓	U-SFPN	60.46 (+1.14)

Table 3: Ablation studies on different upsampling heads on the Pascal Context dataset. Our proposed U-SFPN upsampling head consistently outperforms semantic FPN (SFPN) for both CNN and Transformer backbones.

5.4. Ablation studies on HFGD

In Tab. 4, we conduct ablation studies on each module of our HFGD framework using previously found best configurations in Tab. 1-3. Using all modules together leads to significant accuracy improvement, indicating the effectiveness of the overall architecture.

Backbone	CAE	Upsampling	HFGM	mIOU(%)
ResNet-50	Identity	SFPN	-	47.14
ResNet-50	Ours	SFPN	-	48.76
ResNet-50	Identity	U-SFPN	-	46.99
ResNet-50	Ours	U-SFPN	-	48.67
ResNet-50	Ours	U-SFPN	✓	50.76
Swin-Large	Ours	SFPN	-	56.78
Swin-Large	Identity	U-SFPN	-	58.69
Swin-Large	Ours	U-SFPN	-	55.76
Swin-Large	Ours	U-SFPN	✓	60.46

Table 4: Ablation studies on the proposed three modules using previously found best configurations in Tab. 1-3 on Pascal Context dataset.

5.5. Computational cost of HFGD

The computational cost of our HFGD and two other state-of-the-art methods are listed in Tab. 5. HFGD uses much lower GFLOPs than a similar dilation model (Self-Attention + CAR [15]) but achieves better mIOU (50.76% vs 50.50% [15]). When compared with SemanticFPN, HFGD ($OS = 4$) achieves 3.62% mIOU gain with an affordable extra computation cost (71.63 GFLOPs vs 45.65 GFLOPs).

5.6. Comparison with the state-of-the-art methods

To compare with the state-of-the-art, we adopt ConvNeXt-L as the backbone for our HFGD. We set the

Method	Backbone	GFLOPs	mIOU%
SA (CAR)	ResNet-50 (D8)	158.96	50.50
SemanticFPN	ResNet-50	45.65	47.14
HFGD ($OS=4$)	ResNet-50	71.63	50.76
HFGD ($OS=2$)	ResNet-50	153.62	51.00

Table 5: Computational analysis of HFGD on a $513 \times 513 \times 3$ input image. Previously, although more efficient, upsampling-based methods (e.g. SemanticFPN) cannot produce as accurate results as the dilation-based methods. HFGD ($OS = 4$) closes this accuracy gap while still being efficient. If a similar computation budget is given, HFGD ($OS = 2$) can further improve the accuracy.

Methods	Backbone	Avenue	mIOU(%)	
			SS	MF
SETR* [35]	ViT-L	CVPR'21	-	55.8
DPT* [29]	ViT-Hybrid	ICCV'21	-	60.5
Segmenter* [30]	ViT-L	ICCV'21	-	59.0
OCNet* [49]	HRNet-W48	IJCV'21	-	56.2
CAA* [16]	EfficientNet-B7	AAAI'22	-	60.5
SegNeXt* [11]	MSCAN-L	NIPS'22	59.2	60.9
CAA + CAR [15]	ConvNeXt-L	ECCV'22	62.7	63.9
HFGD ($OS=4$)	ConvNeXt-L	-	63.8	64.9

Table 6: Comparisons to state-of-the-art methods on Pascal Context dataset. Note that methods marked with '*' report mIOU from their papers while the others are obtained with our implementation. *SS*: Single scale performance w/o flipping. *MF*: Multi-scale performance w/ flipping.

training iterations to 40K while all the other training settings are the same as stated in Sec. 4. As shown in Tab. 6, our HFGD achieved 63.8% mIOU with single-scale without flipping and 64.9% mIOU with multi-scales with flipping, outperforming previous state-of-the-art by 1% mIOU in ECCV-2022. HFGD is now the new state-of-the-art method on Pascal Context for the methods that only use the ImageNet pre-trained backbone without extra techniques [36].

5.7. Visualizations on Pascal Context

We present visual comparisons among Self-Attention + CAR (dilation, $OS = 8$), SemanticFPN, and our HFGD. As shown in Fig. 4, HFGD achieves better accuracy than SemanticFPN and contains more details than dilated model (e.g. the last row, the legs of the person).

6. Experiments on COCOStuff164k Dataset

COCOStuff-164k, which becomes popular in recent years, poses a great challenge for semantic segmentation models due to its high diversity (118k training images and

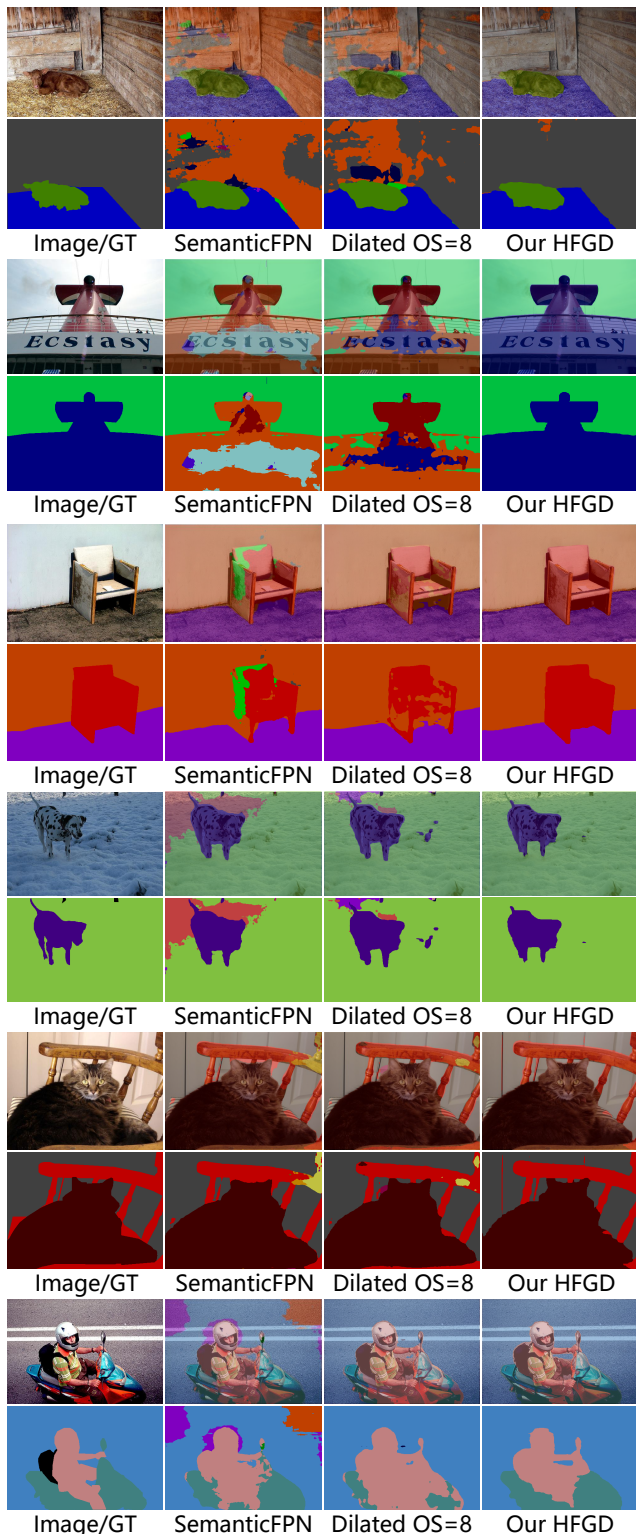


Figure 4: Visual comparisons on Pascal Context between SemanticFPN, Self-Attention + CAR (denoted as “Dilated OS=8”), and our HFGD. All models used ResNet-50 as the backbone. The results are obtained using single-scale without flipping.

Methods	Backbone	Avenue	mIOU(%)	
			SS	MF
OCR* [47, 48]	HRFormer-B	NIPS’21	-	43.3
SegFormer* [44]	MiT-B5	NIPS’21	-	46.7
CAA* [16]	EfficientNet-B5	AAAI’22	-	47.3
SegNeXt* [11]	MSCAN-L	NIPS’22	46.5	47.2
HFGD (OS=4)	ConvNeXt-L	-	49.0	49.4

Table 7: Comparisons to state-of-the-art methods on CO-COStuff164K dataset. Note that methods marked with ‘*’ report mIOU from their papers while the others are obtained with our implementation. *SS*: Single scale performance w/o flipping. *MF*: Multi-scale performance w/ flipping.

Method	Backbone	<i>OS</i>	mIOU(%)
SemanticFPN	ResNet-50	4	76.44
HFGD	ResNet-50	4	79.11
HFGD	ResNet-50	2	79.81 (+0.7)

Table 8: Ablation studies on different output stride modes of U-SFPN on Cityscapes dataset.

5000 testing images) and complexity (171 classes). We adopt ConvNeXt-Large as our backbone network and follow the training settings described in Sec. 4 and we train our model for 40K iterations. In Tab. 7, we compare our proposed HFGD with other state-of-the-art methods. HFGD outperforms the previous state-of-the-art by a large margin (49.4% vs 47.3% mIOU).

7. Experiments on Cityscapes Dataset

Cityscapes is a semantic segmentation dataset that consists of high-resolution images of road scenes with accurate annotations. It has 19 labeled classes and contains 2975/500/1525 training/validation/test images.

7.1. Ablation studies on feature map resolution

We mainly conduct ablation experiments on Cityscapes to verify the superiority of using ultra high resolution feature maps (i.e. $OS = 2$) since its GT annotations are the most accurate. We use ResNet-50 as the backbone and train SemanticFPN, HFGD ($OS = 4$), and HFGD ($OS = 2$) for 30K iterations following the training settings in Sec. 4. As shown in Tab. 8, the $OS = 2$ has further improved the accuracy over $OS = 4$ by 0.7% mIOU (79.11 vs 79.81).

7.2. Comparison with the state-of-the-art methods

To compare our method against the state-of-the-art, we use ConvNeXt-Large and follow the training settings described in Sec. 4. We set the crop size to 513×1025 and train our HFGD model for 60K iterations for the $OS = 4$

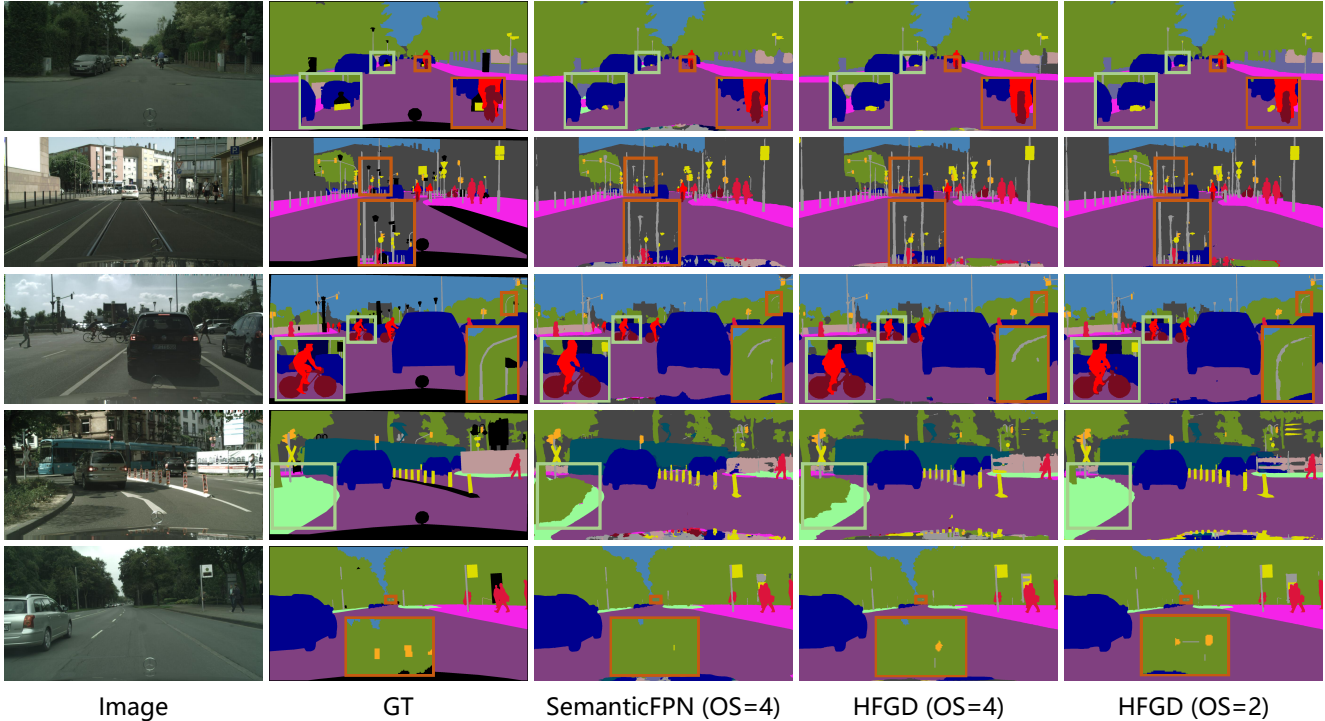


Figure 5: Visual comparisons on Cityscapes between SemanticFPN ($OS = 4$), HFGD ($OS = 4$), and HFGD ($OS = 2$). All models used ResNet-50 as the backbone. The results are obtained using single-scale without flipping.

Methods	Backbone	Avenue	mIOU(%)	
			SS	MF
RepVGG*[7]	RepVGG-B2	CVPR'21	-	80.6
SETR*[44]	ViT-L	CVPR'21	-	82.2
Segmenter*[30]	ViT-L	ICCV'21	-	81.3
OCR*[47, 48]	HRFormer-B	NIPS'21	-	82.6
HRViT-b3*[10]	MiT-B3	CVPR'22	-	83.2
FAN-L*[54]	FAN-Hybrid	ICML'22	-	82.3
SegDeformer*[33]	Swin-L	ECCV'22	-	83.5
HFGD ($OS=4$)	ConvNeXt-L	-	83.1	83.8
HFGD ($OS=2$)	ConvNeXt-L	-	83.2	84.0

Table 9: Comparisons to state-of-the-art methods on Cityscapes dataset. Note that methods marked with ‘*’ report mIOU from their papers while the others are obtained with our implementation. *SS*: Single scale performance w/o flipping. *MF*: Multi-scale performance w/ flipping.

version and 80K iterations for the $OS = 2$ version. As shown in Tab. 9, the proposed HFGD outperforms the previous state-of-the-art proposed in ICML'22 and ECCV'22.

7.3. Visualizations on Cityscapes

We present visual comparisons between SemanticFPN ($OS = 4$) and our HFGD ($OS = 4$ and $OS = 2$) in Fig. 5.

HFGD ($OS = 2$) is clearly more capable of segmenting the small/thin objects. For example, the traffic light in Fig. 5 (last row) is partially missing in $OS=4$, which might be dangerous for automatic vehicles.

8. Conclusion

In this paper, we propose to use the high-level coarse feature to guide the training of the upsampling head (up to $OS = 2$), resulting in an effective and efficient decoder framework. Specifically, HFGD consists of three important components, including HFGM, a context-augmented encoder (CAE), and an upsampling head (U-SFPN), among which CAE and the upsampling head can be upgraded with the latest advancements. With thorough experiments, HFGD achieves largely improved performance over previous upsampling-based state-of-the-art methods (i.e., SemanticFPN [19]) while using much less computation cost than dilated CNNs (e.g. Self-Attention + CAR [15]).

9. Limitation

Theoretically, we could upsample one more time inside U-SFPN, obtaining an $OS = 1$ feature map. However, this increases the computation from 153.62 ($OS = 2$) to 593.77 ($OS = 1$) GFLOPs, which is not affordable. So even more lightweight decoder is required for $OS = 1$.

A. Appendix

A.1. Filter number in SFPN and U-SFPN

For fair comparisons, all the tested SemanticFPN [19] (SFPN) models (in the main paper and this supplementary) use the same number of filters as U-SFPN (i.e. 256).

A.2. HFGD on more backbones

In Tab. 10, We tested more backbones (marked with †) for SemanticFPN and HFGD, including ConvNeXt-L and ConvNeXtV2-L on Pascal Context dataset. The training iteration is set to 30k for the ResNet-50 models using SGD and 40k for the models (i.e. ConvNeXt-L and ConvNeXtV2-L) using AdamW optimizer.

HFGD still brings a gain more than 1% mIOU over SemanticFPN even for a very powerful ConvNeXtV2-L backbone that is pretrained with MAE [12] technique.

Methods	Backbone	Optimizer	mIOU(%)
SemanticFPN	ResNet-50 [13]	SGD	47.1
HFGD	ResNet-50	SGD	50.7 (+3.6)
SemanticFPN†	ConvNeXt-L [24]	AdamW	61.5
HFGD	ConvNeXt-L	AdamW	63.8 (+2.3)
SemanticFPN†	ConvNeXtV2-L [41]	AdamW	63.5
HFGD†	ConvNeXtV2-L	AdamW	64.6 (+1.1)

Table 10: Experiments of HFGD on different backbones. All results are obtained using single-scale without flipping.

A.3. Visualisations on COCO-Stuff-164k dataset

Due to space limit, we present visual comparisons on COCOstuff-164k [1] in Fig. 6. Both SemanticFPN and HFGD (OS=4) use ConvNeXt-L as the backbone and are trained in the same setting. The results are obtained using multi-scale + flipping.

Overall, our HFGD has much better accuracy than SemanticFPN especially on the thin/small objects. For example, SemanticFPN failed to segment the person’s arm (first row in Fig. 6). In the last row of Fig. 6, SemanticFPN missed almost all the birds while our HFGD can correctly locate most of them.

A.4. Future work

The CAE plays an very important role for the final accuracy since its output high-level features is guiding the upsampling branch. Luckily, the extra computation cost is usually limited since we append it after the $OS = 32$ feature maps. So we could probably use the latest modules to further improve the accuracy in the futher.

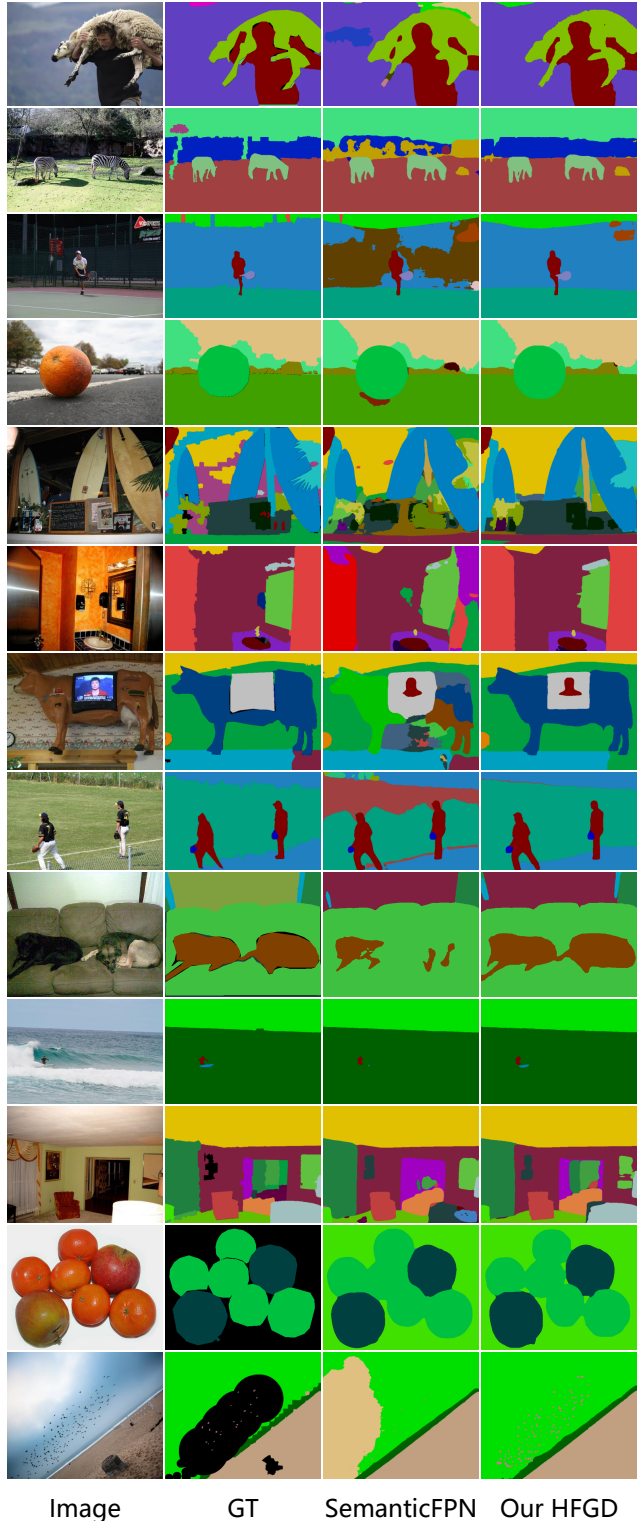


Figure 6: Visual comparisons on COCOstuff-164k between SemanticFPN and our HFGD (OS=4). Black color in the GT indicates the ignored pixels. All models used ConvNeXt-L as the backbone. The results are obtained using multi-scale flipping protocol. Zoom in to see their differences better.

References

- [1] Holger Caesar, Jasper Uijlings, and Vittorio Ferrari. Cocosuff: Thing and stuff classes in context. In *IEEE Conference on Computer Vision and Pattern Recognition*, 2018. 2, 9
- [2] Liang-Chieh Chen, George Papandreou, Iasonas Kokkinos, Kevin Murphy, and Alan L Yuille. Semantic image segmentation with deep convolutional nets and fully connected crfs. In *International Conference on Learning Representations*, 2014. 3
- [3] Liang-Chieh Chen, George Papandreou, Iasonas Kokkinos, Kevin Murphy, and Alan L Yuille. Deeplab: Semantic image segmentation with deep convolutional nets, atrous convolution, and fully connected crfs. *IEEE Transactions on Pattern Analysis and Machine Intelligence*, 2017. 1, 3
- [4] Liang-Chieh Chen, George Papandreou, Florian Schroff, and Hartwig Adam. Rethinking atrous convolution for semantic image segmentation, 2017. 1, 2, 4
- [5] Liang-Chieh Chen, Yukun Zhu, George Papandreou, Florian Schroff, and Hartwig Adam. Encoder-decoder with atrous separable convolution for semantic image segmentation. In *European Conference on Computer Vision*, 2018. 1, 4, 5
- [6] Francois Chollet. Xception: Deep learning with depthwise separable convolutions. In *IEEE Conference on Computer Vision and Pattern Recognition*, 2017. 3
- [7] Xiaohan Ding, Xiangyu Zhang, Ningning Ma, Jungong Han, Guiguang Ding, and Jian Sun. Repvgg: Making vgg-style convnets great again. In *IEEE Conference on Computer Vision and Pattern Recognition*, pages 13733–13742, 2021. 8
- [8] Alexey Dosovitskiy, Lucas Beyer, Alexander Kolesnikov, Dirk Weissenborn, Xiaohua Zhai, Thomas Unterthiner, Mostafa Dehghani, Matthias Minderer, Georg Heigold, Sylvain Gelly, Jakob Uszkoreit, and Neil Houlsby. An image is worth 16x16 words: Transformers for image recognition at scale. In *International Conference on Learning Representations*, 2021. 3
- [9] Jun Fu, Jing Liu, Haijie Tian, Yong Li, Yongjun Bao, Zhe-wei Fang, and Hanqing Lu. Dual attention network for scene segmentation. In *IEEE Conference on Computer Vision and Pattern Recognition*, 2019. 1, 3
- [10] Jiaqi Gu, Hyoukjun Kwon, Dilin Wang, Wei Ye, Meng Li, Yu-Hsin Chen, Liangzhen Lai, Vikas Chandra, and David Z. Pan. Multi-scale high-resolution vision transformer for semantic segmentation. In *IEEE Conference on Computer Vision and Pattern Recognition*, 2022. 8
- [11] Meng-Hao Guo, Cheng-Ze Lu, Qibin Hou, Zheng-Ning Liu, Ming-Ming Cheng, and Shi-Min Hu. Segnext: Rethinking convolutional attention design for semantic segmentation. In *Conference on Neural Information Processing Systems*, 2022. 6, 7
- [12] Kaiming He, Xinlei Chen, Saining Xie, Yanghao Li, Piotr Dollár, and Ross Girshick. Masked autoencoders are scalable vision learners. In *IEEE Conference on Computer Vision and Pattern Recognition*, 2022. 9
- [13] Kaiming He, Xiangyu Zhang, Shaoqing Ren, and Jian Sun. Deep residual learning for image recognition. In *IEEE Conference on Computer Vision and Pattern Recognition*, 2016. 3, 9
- [14] Jonathan Ho, Nal Kalchbrenner, Dirk Weissenborn, and Tim Salimans. Axial attention in multidimensional transformers, 2019. 4
- [15] Ye Huang, Di Kang, Liang Chen, Xuefei Zhe, Wenjing Jia, Linchao Bao, and Xiangjian He. Car: Class-aware regularizations for semantic segmentation. In *European Conference on Computer Vision*, 2022. 1, 2, 4, 6, 8
- [16] Ye Huang, Di Kang, Wenjing Jia, Xiangjian He, and Liu liu. Channelized axial attention - considering channel relation within spatial attention for semantic segmentation. In *AAAI*, 2022. 1, 2, 4, 6, 7
- [17] Ye Huang, Qingqing Wang, Wenjing Jia, and Xiangjian He. See more than once—kernel-sharing atrous convolution for semantic segmentation. *Neuro Computing*, 2021. 1, 2
- [18] Zilong Huang, Xinggang Wang, Yunchao Wei, Lichao Huang, Humphrey Shi, Wenyu Liu, and Thomas S. Huang. Ccnet: Criss-cross attention for semantic segmentation. *IEEE Transactions on Pattern Analysis and Machine Intelligence*, 2020. 1, 2
- [19] Alexander Kirillov, Ross Girshick, Kaiming He, and Piotr Dollar. Panoptic feature pyramid networks. In *IEEE Conference on Computer Vision and Pattern Recognition*, 2019. 2, 3, 5, 8, 9
- [20] Alexander Kirillov, Kaiming He, Ross Girshick, Carsten Rother, and Piotr Dollar. Panoptic segmentation. In *IEEE Conference on Computer Vision and Pattern Recognition*, 2019. 3
- [21] Xia Li, Zhisheng Zhong, Jianlong Wu, Yibo Yang, Zhouchen Lin, and Hong Liu. Expectation-maximization attention networks for semantic segmentation. In *International Conference on Computer Vision*, 2019. 1
- [22] Tsung-Yi Lin, Piotr Dollá, Ross Girshick, Kaiming He, Bharath Hariharan, and Serge Belongie. Feature pyramid networks for object detection. In *IEEE Conference on Computer Vision and Pattern Recognition*, 2017. 2, 3
- [23] Ze Liu, Yutong Lin, Yue Cao, Han Hu, Yixuan Wei, Zheng Zhang, Stephen Lin, and Baining Guo. Swin transformer: Hierarchical vision transformer using shifted windows. In *ICCV*, 2021. 3, 5
- [24] Zhuang Liu, Hanzi Mao, Chao-Yuan Wu, Christoph Feichtenhofer, Trevor Darrell, and Saining Xie. A convnet for the 2020s. In *IEEE Conference on Computer Vision and Pattern Recognition*, 2022. 3, 5, 9
- [25] Jonathan Long, Evan Shelhamer, and Trevor Darrell. Fully convolutional networks for semantic segmentation. In *IEEE Conference on Computer Vision and Pattern Recognition*, 2015. 1
- [26] Cordts Marius, Omran Mohamed, Ramos Sebastian, Rehfeld Timo, Enzweiler Markus, Benenson Rodrigo, Franke Uwe, Stefan Roth, and Schiele Bernt. The cityscapes dataset for semantic urban scene understanding. In *IEEE Conference on Computer Vision and Pattern Recognition*, 2016. 2
- [27] Tan Mingxing and Le Quoc. Efficientnet: Rethinking model scaling for convolutional neural networks. In *International Conference on Machine Learning*, 2019. 3
- [28] Roozbeh Mottaghi, Xianjie Chen, Xiaobai Liu, Nam-Gyu Cho, Seong-Whan Lee, Sanja Fidler, Raquel Urtasun, and

- Alan Yuille. The role of context for object detection and semantic segmentation in the wild. In *IEEE Conference on Computer Vision and Pattern Recognition*, 2014. 2
- [29] René Ranftl, Alexey Bochkovskiy, and Vladlen Koltun. Vision transformers for dense prediction. In *ICCV*, 2021. 6
- [30] Strudel Robin, Garcia Ricardo, Laptev Ivan, and Schmid Cordelia. Segmenter: Transformer for semantic segmentation. In *ICCV*, 2021. 6, 8
- [31] Olaf Ronneberger, Philipp Fischer, and Thomas Brox. U-net: Convolutional networks for biomedical image segmentation. In *MICCAI*, 2015. 1, 2, 3
- [32] Mark Sandler, Andrew Howard, Menglong Zhu, Andrey Zhmoginov, and Liang-Chieh Chen. Mobilenetv2: Inverted residuals and linear bottlenecks. In *IEEE Conference on Computer Vision and Pattern Recognition*, 2018. 3
- [33] Bowen Shi, Dongsheng Jiang, Xiaopeng Zhang, Han Li, Wenrui Dai, Junni Zou, Hongkai Xiong, and Qi Tian. A transformer-based decoder for semantic segmentation with multi-level context mining. In *European Conference on Computer Vision*, 2022. 8
- [34] K. Simonyan and A. Zisserman. Very deep convolutional networks for large-scale image recognition. In *International Conference on Learning Representations*, 2015. 3
- [35] Zheng Sixiao, Lu Jiachen, Zhao Hengshuang, Zhu Xiatian, Luo Zekun, Wang Yabiao, Fu Yanwei, Feng Jianfeng, Xiang Tao, Torr Philip H.S., and Zhang Li. Rethinking semantic segmentation from a sequence-to-sequence perspective with transformers. In *IEEE Conference on Computer Vision and Pattern Recognition*, 2021. 6
- [36] Andreas Peter Steiner, Alexander Kolesnikov, Xiaohua Zhai, Ross Wightman, Jakob Uszkoreit, and Lucas Beyer. How to train your vit? data, augmentation, and regularization in vision transformers. *Transactions on Machine Learning Research*, 2022. 2, 6
- [37] Ashish Vaswani, Noam Shazeer, Niki Parmar, Jakob Uszkoreit, Llion Jones, Aidan N. Gomez, Łukasz Kaiser, and Illia Polosukhin. Attention is all you need. In *Conference on Neural Information Processing Systems*, 2017. 4
- [38] Huiyu Wang, Yukun Zhu, Bradley Green, Hartwig Adam, Alan Yuille, and Liang-Chieh Chen. Axial-deeplab: Stand-alone axial-attention for panoptic segmentation. In *European Conference on Computer Vision*, 2020. 4
- [39] Jingdong Wang, Ke Sun, Tianheng Cheng, Borui Jiang, Chaorui Deng, Yang Zhao, Dong Liu, Yadong Mu, Mingkui Tan, Xinggang Wang, Wenyu Liu, and Bin Xiao. Deep high-resolution representation learning for visual recognition. *IEEE Transactions on Pattern Analysis and Machine Intelligence*, 2020. 3
- [40] Xiaolong Wang, Ross Girshick, Abhinav Gupta, and Kaiming He. Non-local neural networks. In *IEEE Conference on Computer Vision and Pattern Recognition*, 2018. 2, 3, 4, 5
- [41] Sanghyun Woo, Shoubhik Debnath, Ronghang Hu, Xinlei Chen, Zhuang Liu, In So Kweon, and Saining Xie. Convnext v2: Co-designing and scaling convnets with masked autoencoders. In *IEEE Conference on Computer Vision and Pattern Recognition*, 2023. 9
- [42] Huikai Wu, Junge Zhang, Kaiqi Huang, Kongming Liang, and Yu Yizhou. Fastfcn: Rethinking dilated convolution in the backbone for semantic segmentation, 2019. 3
- [43] Tete Xiao, Yingcheng Liu, Bolei Zhou, Yuning Jiang, and Jian Sun. Unified perceptual parsing for scene understanding. In *European Conference on Computer Vision*, 2018. 1, 3
- [44] Enze Xie, Wenhai Wang, Zhiding Yu, Anima Anandkumar, Jose M Alvarez, and Ping Luo. Segformer: Simple and efficient design for semantic segmentation with transformers. In *Conference on Neural Information Processing Systems*, 2021. 1, 7, 8
- [45] Maoge Yang, Kun Yu, Chi Zhang, Zhiwei Li, and Kuiyuan Yang. Denseaspp for semantic segmentation in street scenes. In *IEEE Conference on Computer Vision and Pattern Recognition*, 2018. 1
- [46] Fisher Yu and Vladlen Koltun. Multi-scale context aggregation by dilated convolutions. In *International Conference on Learning Representations*, 2016. 3
- [47] Yuhui Yuan, Xilin Chen, and Jingdong Wang. Object-contextual representations for semantic segmentation. In *European Conference on Computer Vision*, 2020. 4, 5, 7, 8
- [48] Yuhui Yuan, Rao Fu, Lang Huang, Weihong Lin, Chao Zhang, Xilin Chen, and Jingdong Wang. Hrformer: High-resolution transformer for dense prediction. In *Conference on Neural Information Processing Systems*, 2021. 7, 8
- [49] Yuhui Yuan, Lang Huang, Jianyuan Guo, Chao Zhang, Xilin Chen, and Jingdong Wang. Ocnet: Object context network for scene parsing. *International Journal of Computer Vision*, 2021. 2, 6
- [50] Hang Zhang, Kristin Dana, Jianping Shi, Zhongyue Zhang, Xiaoang Wang, Amrith Tyagi, and Amit Agrawal. Context encoding for semantic segmentation. In *IEEE Conference on Computer Vision and Pattern Recognition*, 2018. 1
- [51] Hang Zhang, Chongruo Wu, Zhongyue Zhang, Yi Zhu, Zhi Zhang, Haibin Lin, Yue Sun, Tong He, Jonas Muller, R. Manmatha, Mu Li, and Alexander Smola. Resnest: Split-attention networks. *arXiv preprint arXiv:2004.08955*, 2020. 3
- [52] Hang Zhang, Han Zhan, Chenguang Wang, and Junyuan Xie. Semantic correlation promoted shape-variant context for segmentation. In *IEEE Conference on Computer Vision and Pattern Recognition*, 2019. 1, 4
- [53] Hengshuang Zhao, Jianping Shi, Xiaojuan Qi, Xiaoang Wang, and Jiaya Jia. Pyramid scene parsing network. In *IEEE Conference on Computer Vision and Pattern Recognition*, 2017. 1, 3, 4
- [54] Daquan Zhou, Zhiding Yu, Enze Xie, Chaowei Xiao, Anima Anandkumar, Jiashi Feng, and Jose M. Alvarez. Understanding the robustness in vision transformers. In *International Conference on Machine Learning*, 2022. 8
- [55] Zhen Zhu, Mengde Xu, Song Bai, Tengeng Huang, and Xiang Bai. Asymmetric non-local neural networks for semantic segmentation. In *International Conference on Computer Vision*, 2019. 1, 2